Article

Global-scale human impact on delta morphology has led to net land area gain

J. H. Nienhuis[1,2,3,4]*, A. D. Ashton[5], D. A. Edmonds[6], A. J. F. Hoitink[3], A. J. Kettner[7], J. C. Rowland[8] & T. E. Törnqvist[4]

River deltas rank among the most economically and ecologically valuable environments on Earth. Even in the absence of sea-level rise, deltas are increasingly vulnerable to coastal hazards as declining sediment supply and climate change alter their sediment budget, affecting delta morphology and possibly leading to erosion[1–3]. However, the relationship between deltaic sediment budgets, oceanographic forces of waves and tides, and delta morphology has remained poorly quantified. Here we show how the morphology of about 11,000 coastal deltas worldwide, ranging from small bayhead deltas to mega-deltas, has been affected by river damming and deforestation. We introduce a model that shows that present-day delta morphology varies across a continuum between wave (about 80 per cent), tide (around 10 per cent) and river (about 10 per cent) dominance, but that most large deltas are tide- and river-dominated. Over the past 30 years, despite sea-level rise, deltas globally have experienced a net land gain of 54 ± 12 square kilometres per year (2 standard deviations), with the largest 1 per cent of deltas being responsible for 30 per cent of all net land area gains. Humans are a considerable driver of these net land gains—25 per cent of delta growth can be attributed to deforestation-induced increases in fluvial sediment supply. Yet for nearly 1,000 deltas, river damming[4] has resulted in a severe (more than 50 per cent) reduction in anthropogenic sediment flux, forcing a collective loss of 12 ± 3.5 square kilometres per year (2 standard deviations) of deltaic land. Not all deltas lose land in response to river damming: deltas transitioning towards tide dominance are currently gaining land, probably through channel infilling. With expected accelerated sea-level rise[5], however, recent land gains are unlikely to be sustained throughout the twenty-first century. Understanding the redistribution of sediments by waves and tides will be critical for successfully predicting human-driven change to deltas, both locally and globally.

River damming and land-use change affect the sediment supply to deltas, and can lead to substantial physical transformations of the coastal landscape. Existing attempts to predict delta morphology are conceptually rich but often qualitative[6–11]. Most prominently, Galloway[7] introduced a process-based ternary diagram, hypothesizing that delta morphology reflects the relative importance of wave, tide and river forcing. However, the lack of a quantitative prediction of delta morphology for a given relative influence of each forcing has prevented direct application of this foundational ternary diagram to understanding delta form. For example, how does decreased sediment supply affect deltas and how can this translate into land gain or land loss? A fundamental limitation in predicting delta change has been the poor understanding of how sediment supply has shaped modern delta morphology itself, motivating our development of an a priori theory of the controls of delta morphology.

A new model for delta change

On the basis of two recent quantitative studies[12,13], we here introduce a ternary diagram that allows prognosis of delta morphology and morphologic change using sediment fluxes (Fig. 1a). We apply this approach on a global scale. First, we predict delta morphology for conditions that resemble a world without substantial human impact on the fluvial sediment supply. Next, we compare these predictions to the delta morphology that is expected on the basis of recent modifications to sediment fluxes due to both deforestation and river damming.

[1]Department of Physical Geography, Utrecht University, Utrecht, The Netherlands. [2]Department of Earth, Ocean, and Atmospheric Sciences, Florida State University, Tallahassee, FL, USA. [3]Environmental Sciences, Wageningen University and Research, Wageningen, The Netherlands. [4]Department of Earth and Environmental Sciences, Tulane University, New Orleans, LA, USA. [5]Department of Geology and Geophysics, Woods Hole Oceanographic Institution, Woods Hole, MA, USA. [6]Department of Earth and Atmospheric Sciences, Indiana University, Bloomington, IN, USA. [7]Institute of Arctic and Alpine Research, University of Colorado, Boulder, CO, USA. [8]Earth & Environmental Sciences Division, Los Alamos National Laboratory, Los Alamos, NM, USA. *e-mail: j.h.nienhuis@uu.nl
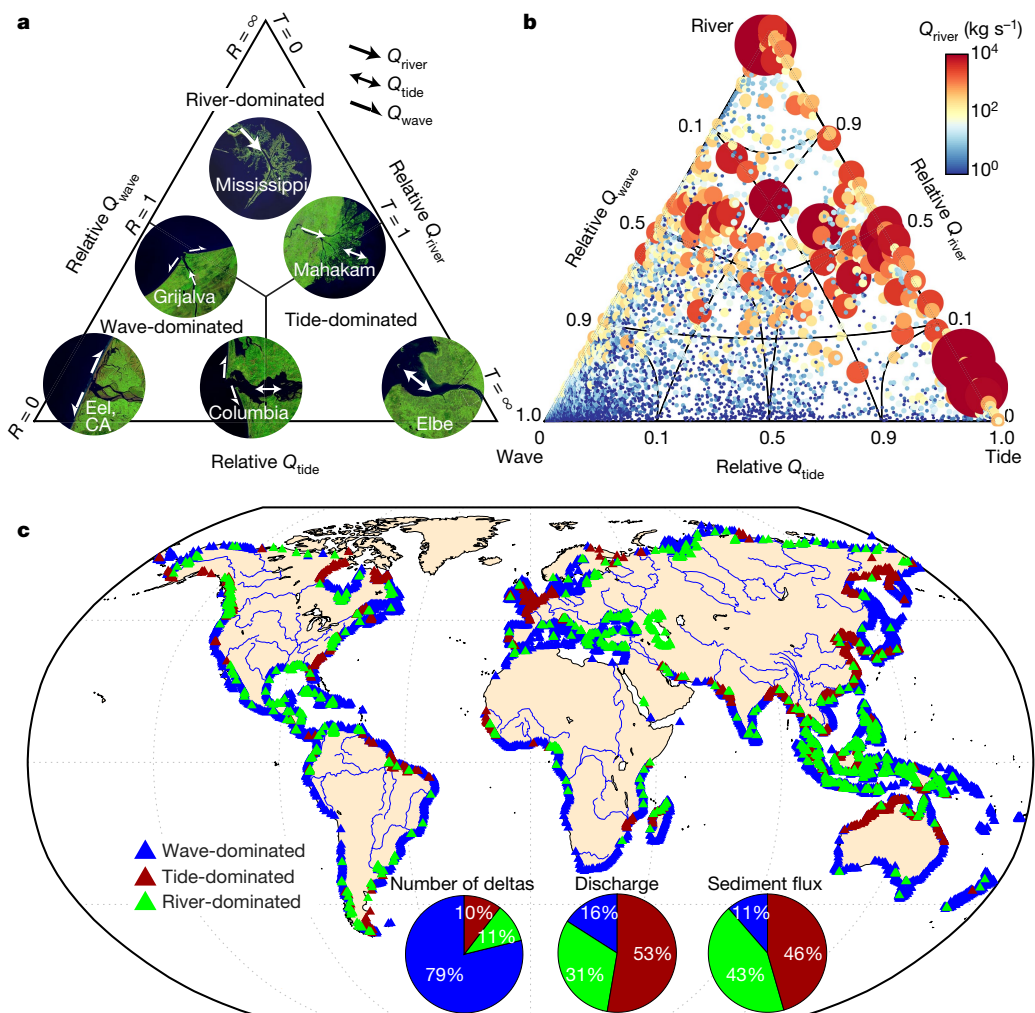
Fig. 1 | Global distribution of predicted pristine delta morphologies.
a, Galloway[7] ternary diagram, recast to show the relative sediment fluxes Q_{wave}, Q_{tide} and Q_{river} (see Methods). Insets are satellite images of representative delta morphologies, with arrows highlighting the predicted direction and magnitude of sediment fluxes. Map imagery in Figs. 1, 3 and Extended Data Fig. 5 from NASA, Google Earth, TerraMetrics, 2019. **b**, Prediction of pristine (Q_{river}^{p}) morphology of 10,848 deltas sized and coloured by fluvial sediment flux. Axes follow a sigmoidal, rather than linear, function to better illustrate the distribution of strongly wave-, river- or tide-dominated deltas. **c**, Global geographic distribution of predicted pristine delta morphologies (see .kml file at https://doi.org/10.17605/OSF.IO/S28QB). Plots in Figs. 1–3 and Extended Data Figs. 1–5 generated by Matlab 2018b (https://mathworks.com/products/matlab.html).

We distinguish between two formative values of the fluvial sediment supply (Q_{river}, in kilograms per second), representing pristine sediment fluxes before substantial anthropogenic influences (Q_{river}^{p}) and contemporary ('disturbed') sediment fluxes accounting for dam construction and land-use change in the contributing drainage basins (Q_{river}^{d})[14]. Because deltas respond to sediment flux changes over timespans of decades to centuries[15], our delta morphology predictions based on Q_{river}^{d} correspond to a future equilibrium state towards which deltas are currently evolving. Using observations of delta land area changes in 1985–2015, we can investigate how much humans have changed deltas and how deltas may change in the future.

Our ternary diagram compares the fluvial sediment supply to tide- and wave-driven sediment fluxes near the river mouth. First, in the absence of tides, a delta is expected to attain a wave-dominated, triangular shape if the potential for waves to move sediment away from the river mouth (Q_{wave}, in kilograms per second; see Methods) exceeds the delivered fluvial sediment flux (Q_{river}). Importantly, Q_{river} and Q_{wave} enable predictions independent of the observed delta morphology and allow these sediment fluxes to be used for delta change forecasting. The ratio Q_{river}/Q_{wave} (termed the fluvial dominance ratio, R) indicates whether a delta does not deflect the coastline ($R \approx 0$; for example, Eel; Fig. 1a),

has a roughly triangular shape with a shoreline angle between 0° and 45° ($0 < R < 1$; for example, Grijalva), or is river-dominated ($R > 1$; for example, Mississippi). Increases in R lead to increased deposition near the river mouth, whereas decreases in R can result in distal shoreline progradation even as the river mouth erodes[12].

In the absence of waves, delta morphology is determined by the competition between river discharge and tidal flows. Morphologically, tidal dominance manifests itself as a seaward widening of the channel banks[13,16]. By contrast, river-dominated delta channels have an approximately constant width. The tidal dominance ratio T, as originally defined[13], relates the tidal discharge amplitude to the mean fluvial discharge. Here we use T as a ratio of sediment fluxes and define a tidal sediment flux (Q_{tide}, in kilograms per second) along with a fluvial sediment flux (Q_{river}, in kilograms per second) (Fig. 1a, Methods). If $T < 1$, the delta is river-dominated and there is no flow reversal in the deltaic channel(s). If $T > 1$, the delta is tide-dominated and the widened deltaic channel(s), or some portion thereof, experience(s) flow reversal. Changes in T will affect delta channels; for example, a decrease in fluvial sediment flux (Q_{river}) will cause the channel to infill and narrow[13].

Our ternary diagram represents the relative contribution of Q_{tide}, Q_{river} and Q_{wave}, and therefore also two morphological attributes of a
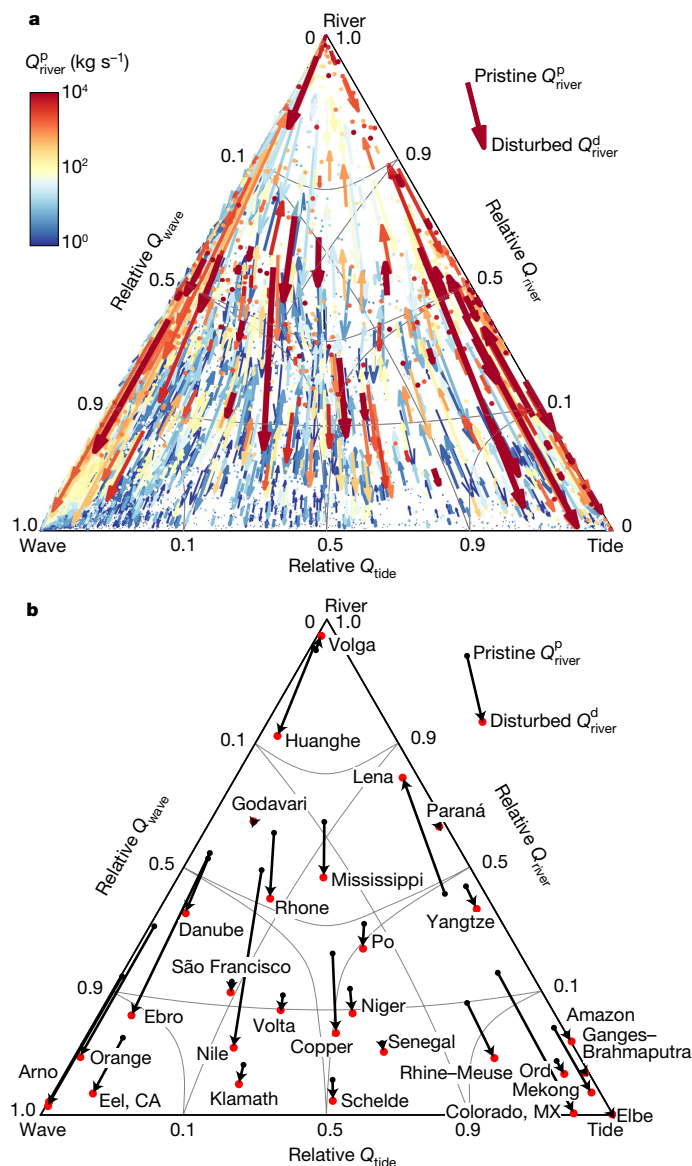
Fig. 2 | Predicted delta morphologic change from pristine to future equilibrium conditions. a, Arrows indicate the direction and magnitude of the predicted change. Colour and thickness indicate the pristine fluvial sediment flux. b, Predicted anthropogenically driven morphologic change for a selection of well-known deltas. See also Extended Data Table 4.

delta: the seaward divergence of the channel banks and the shoreline protrusion angle (Fig. 1a). It allows us to explore delta morphologies that arise from varying Q_{tide}, Q_{river} and Q_{wave}, including the expected morphology of deltas near the limit of low fluvial sediment flux, now or in the future[17]. Deltas near this limit are often referred to as strand-plains (for example, São Francisco[18]) or alluvial estuaries (for example, Elbe[8]). Here we show that this wide variety of coastal morphologies with different sizes lies along a continuum that can be characterized by the relative balance of these three sediment fluxes. For simplicity, we therefore refer to all morphologies within our ternary diagram as deltas—a broader definition compared to other studies[19].

A global assessment of delta change

To predict pristine delta morphology globally, we determined the location of coastal deltas worldwide ($n = 10,848 \pm 494$; 2 s.d.) and calculated pristine river-, wave- and tide-driven sediment fluxes. These fluxes
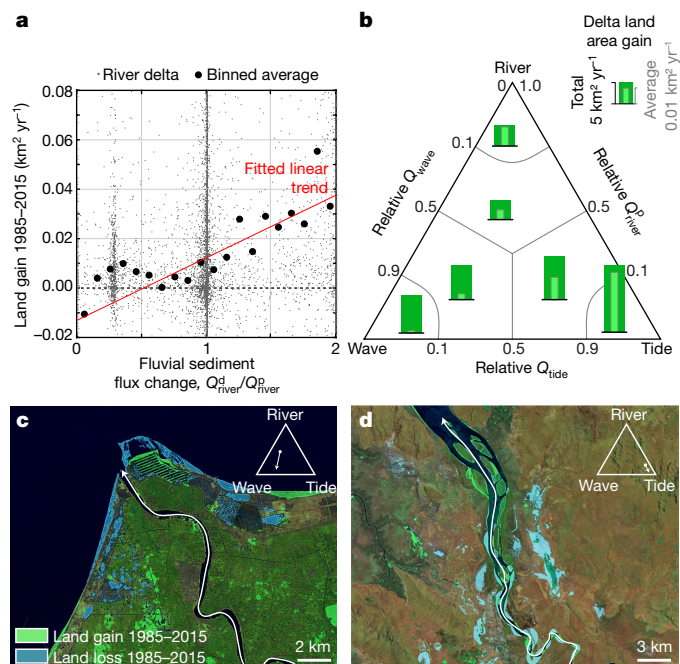

Fig. 3 | Rates and drivers of delta land area change over the period 1985–2015. a, b, Land area change rates related to changes in the fluvial sediment supply (a) and pristine delta morphology (b). c, d, Land change in the Nile Delta, Egypt (c) and the Ord River Delta, Australia (d). Map imagery, NASA, Google Earth, TerraMetrics, 2019 and ref. [20]. The inset diagrams indicate the predicted morphologic change.

occur in all combinations, and the predicted delta morphologies vary across a continuum between wave, tide and river dominance, as tested against observed morphologies (see Methods). Most deltas are wave-dominated (~79% ± 9%; 2 s.d.); however, large deltas ($Q_{river}^{p} > 50$ kg s^{-1}, $n = 701$) are predominantly (68%) river- or tide-dominated (Fig. 1b), owing to their large fluvial sediment flux and their low-gradient delta plains (5×10^{-4} versus 3×10^{-3} for all deltas on average), making them conducive to large tidal sediment fluxes[13]. River- and tide-dominated deltas are associated with 83% of the modern fluvial discharge and 87% of the modern sediment flux to the global ocean.

A comparison of equilibrium predictions for pristine and disturbed sediment fluxes shows the extent to which humans are likely to be modifying delta morphology by influencing river discharge and sediment fluxes. In total, 970 deltas have had their fluvial sediment supply reduced by >50%, collectively from ~9×10^{4} kg s^{-1} to ~2×10^{4} kg s^{-1}, resulting in a shift towards wave or tide dominance (Fig. 2a). On the other hand, human-driven soil erosion, mostly through deforestation, is predicted to have caused a >50% increase in sediment flux, or ~5×10^{4} kg s^{-1}, to ~1,500 deltas. We predict that sediment supply changes are forcing considerable ongoing adjustments in the shoreline protrusion and channel width of many well-known deltas (Fig. 2b).

Next, we use the Aqua Monitor[20] to investigate how our predicted ongoing morphologic change is reflected in recent delta surface area change (see Methods). We find that over the past 30 years, deltas globally have gained 181 ± 8.3 km^2 yr^{-1} and lost 127 ± 8.3 km^2 yr^{-1}, resulting in a net gain of 54 ± 11.8 km^2 yr^{-1} (2 s.d.). With a combined ~9×10^9 m^3 yr^{-1} fluvial sediment flux to the global ocean[21], deltas on average require 150 m^3 of sediment delivered to the coast for every square metre of land gain. Delta growth is particularly pronounced for tide-dominated deltas, representing 46% of the net land gain.

We find that humans have measurably altered delta growth rates globally (Fig. 3a, Table 1). Human-induced changes to the fluvial sediment flux ($Q_{river}^{d} - Q_{river}^{p}$) explain 16% of the recent delta land area

Table 1 | Global delta morphology and morphodynamic change

	Number of deltas	Total Q_{river}^{p} (kg s^{-1})	Total Q_{river}^{d} (kg s^{-1})	Land gain (km^2 yr^{-1})	Land loss (km^2 yr^{-1})	Net land gain (km^2 yr^{-1})
Wave-dominated	8,552	6.0×10^4	5.9×10^4	35 ± 7	-17 ± 7	19 ± 10
River-dominated	1,169	20×10^4	15×10^4	49 ± 3	-39 ± 3	10 ± 4
Tide-dominated	1,127	22×10^4	22×10^4	97 ± 3	-72 ± 3	25 ± 4
Fluvial flux decrease (>50%)	970	9.2×10^4	1.8×10^4	15 ± 3	-27 ± 3	-12 ± 4
Fluvial flux increase (>50%)	1,478	3.1×10^4	7.6×10^4	36 ± 3	-11 ± 3	25 ± 4
Tidal reworking[a]	234	4.2×10^4	1.0×10^4	2 ± 1	-1 ± 1	0.9 ± 1
Wave reworking[b]	736	5.0×10^4	0.8×10^4	12 ± 2	-25 ± 2	-13 ± 3
Largest 1%	108	35×10^4	29×10^4	103 ± 1	-88 ± 1	15 ± 1
Largest 10%	1,085	46×10^4	40×10^4	143 ± 3	-109 ± 3	34 ± 4
Largest 100% (all deltas)	10,848	49×10^4	43×10^4	181 ± 8	-127 ± 8	54 ± 12

Error limits indicate 2 s.d.
[a]Tidal reworking defined as a fluvial sediment flux decrease greater than 50% and $Q_{wave} < Q_{tide}$.
[b]Wave reworking defined as a fluvial sediment flux decrease greater than 50% and $Q_{wave} > Q_{tide}$.

changes ($P = 0$). Deforestation has led to land gain, thus far exceeding land loss due to river dams. Delta change is most pronounced in South, Southeast and East Asia, where 57% of all new deltaic land is gained and 61% of all delta land loss occurs. North America, owing to the rapid decline of the Mississippi Delta, partly due to damming[22], is the only continent with a net decrease in deltaic area (Extended Data Table 3).

Delta response to river damming depends on how waves and tides redistribute (rework) deltaic sediment (Fig. 3b). Two dominant patterns emerge. Deltas that are predicted to become more wave-dominated are, on average, eroding (Table 1). Morphologically, this change is expected because wave reworking of the delta near the river mouth results in erosion[23] (Fig. 3c). However, tidally influenced deltas that face markedly reduced fluvial sediment supply are slightly gaining (or not necessarily losing) land area (Table 1, Fig. 3d). This counterintuitive result is caused by the infilling of deltaic channels[13]. In contrast to some studies (for example, in the Amazon[24] or Yangtze[25]) that assume that dams will lead to delta erosion, our analysis suggests that tides can overcompensate for the reduced fluvial discharge or sediment input and increase landward sediment transport. Increased landward transport probably results from the relative enhancement of tidal flood flow in cases where fluvial discharge (peaks) are decreasing[26,27] and comes at the expense of the extensive subaqueous delta.

Discussion

Because our predictions of delta morphologic change are global in scale, they exclude various processes affecting deltas now and in the future, such as relative sea-level change and direct anthropogenic modification—processes included in measurements of land area change. For heavily modified delta plains (for example, the Rhine–Meuse Delta), morphologic predictions based on changes in the fluvial sediment flux can indicate long-term system tendencies; however, the actual response will most probably involve direct human–delta interactions not considered by our approach.

Our ternary diagram simplifies delta morphology into two shape metrics: delta protrusion angle and channel width. It therefore differs from earlier, qualitative work. For example, the São Francisco river is often thought of as having an end-member wave-dominated delta[7]. Here we show that the delta is wave-dominated, but that fluvial sediment has created a substantial shoreline protrusion ($R \approx 0.3$) and that tides probably create flow reversal at the river mouth ($T \approx 1$). We note also that two deltas that are placed near each other in our framework (for example, Volga and Huanghe; Fig. 2b) might be considered to be different on the basis of other aspects of delta morphology (for example, shoreline rugosity, number of distributary channels). Our ternary diagram can help explore the origin of such morphologic differences.

For example, Q_{river} is split across distributary channels, whereas Q_{wave} and Q_{tide} act on each river mouth. Via channel bifurcation, deltas that are marginally river-dominated can therefore transition towards wave or tide dominance[12]. Conversely, because Q_{wave} suppresses channel bifurcation[28], we could potentially predict the number of distributary channels for river deltas.

Changes to sediment fluxes explain dominant trends in delta planform evolution and are sufficiently general to allow for coupling with other processes. Sea-level rise and subsidence, for example, tend to increase deltaic channel and topset aggradation[29], which would reduce fluvial sediment supply to the river mouth (Q_{river}) and result in a relative increase of wave and tide dominance. Other controls on delta morphology, such as grain size or wave climate changes[30], can be incorporated into our model, but appropriate data for global applications are currently lacking. For example, grain size is inversely correlated to Q_{tide} and Q_{wave} (refs. [12,13]), making coarser-grained deltas more likely to be river-dominated.

In conclusion, we can successfully predict large-scale delta morphology and we find that human intervention in drainage basins has had a considerable global effect. The recent reductions in sediment supply explain important patterns of land loss in cases where waves take over. Yet on a global scale, land gains resulting from deforestation exceed losses due to river damming. In the future, however, dam emplacement and sand mining is projected to accelerate in developing nations, further lowering fluvial sediment supply to river deltas[31,32]. Sea-level rise and land subsidence rates are increasing in many deltas[5,33,34]. Future predictions of delta morphology therefore will need to consider further diminished sediment loads and higher relative sea-level rise rates.

Online content

Any methods, additional references, Nature Research reporting summaries, source data, extended data, supplementary information, acknowledgements, peer review information; details of author contributions and competing interests; and statements of data and code availability are available at https://doi.org/10.1038/s41586-019-1905-9.

1. Syvitski, J. P. M. et al. Sinking deltas due to human activities. *Nat. Geosci.* **2**, 681–686 (2009).
2. Tessler, Z. D. et al. Profiling risk and sustainability in coastal deltas of the world. *Science* **349**, 638–643 (2015).
3. Pelletier, J. D. et al. Forecasting the response of Earth's surface to future climatic and land use changes: A review of methods and research needs. *Earths Future* **3**, 220–251 (2015).
4. Syvitski, J. P. M. & Kettner, A. Sediment flux and the Anthropocene. *Philos. Trans. R. Soc. A* **369**, 957–975 (2011).
5. Nerem, R. S. et al. Climate-change–driven accelerated sea-level rise detected in the altimeter era. *Proc. Natl Acad. Sci. USA* **115**, 2022–2025 (2018).

Article

6. Wright, L. D. & Coleman, J. M. Variations in morphology of major river deltas as functions on ocean wave and river discharge regimes. *Am. Assoc. Pet. Geol. Bull.* **57**, 370–398 (1973).
7. Galloway, W. D. in *Deltas, Models for Exploration* (ed. Broussard, M. L.) 86–98 (Houston Geological Society, 1975).
8. Boyd, R., Dalrymple, R. & Zaitlin, B. A. Classification of clastic coastal depositional environments. *Sedim. Geol.* **80**, 139–150 (1992).
9. Orton, G. J. & Reading, H. G. Variability of deltaic processes in terms of sediment supply, with particular emphasis on grain size. *Sedimentology* **40**, 475–512 (1993).
10. Bhattacharya, J. P. in *Facies Models Revisited* (eds Posamentier, H. W. & Walker, R. G.) 237–292 (Society for Sedimentary Geology, 2006).
11. Leeder, M. R. *Sedimentology and Sedimentary Basins: From Turbulence to Tectonics* (Wiley-Blackwell, 2011).
12. Nienhuis, J. H., Ashton, A. D. & Giosan, L. What makes a delta wave-dominated? *Geology* **43**, 511–514 (2015).
13. Nienhuis, J. H., Hoitink, A. J. F. & Törnqvist, T. E. Future change to tide-influenced deltas. *Geophys. Res. Lett.* **45**, 3499–3507 (2018).
14. Cohen, S., Kettner, A. J. & Syvitski, J. P. M. Global suspended sediment and water discharge dynamics between 1960 and 2010: continental trends and intra-basin sensitivity. *Global Planet. Change* **115**, 44–58 (2014).
15. Swenson, J. B. Relative importance of fluvial input and wave energy in controlling the timescale for distributary-channel avulsion. *Geophys. Res. Lett.* **32**, L23404 (2005).
16. Langbein, W. B. The hydraulic geometry of a shallow estuary. *Int. Assoc. Sci. Hydrol. Bull.* **8**, 84–94 (1963).
17. Dalrymple, R. W. in *Facies Models: Response to Sea Level Change* (eds Walker, R. G. & James, N. P.) 195–218 (Geological Association of Canada, 1992).
18. Dominguez, J. M. L. The São Francisco strandplain: a paradigm for wave-dominated deltas? *Geol. Soc. Lond. Spec. Publ.* **117**, 217–231 (1996).
19. Caldwell, R. L. et al. A global delta dataset and the environmental variables that predict delta formation on marine coastlines. *Earth Surf. Dyn.* **7**, 773–787 (2019).
20. Donchyts, G. et al. Earth's surface water change over the past 30 years. *Nat. Clim. Change* **6**, 810–813 (2016).
21. Syvitski, J. P. M., Vörösmarty, C. J., Kettner, A. J., & Green, P. Impact of humans on the flux of terrestrial sediment to the global coastal ocean. *Science* **308**, 376–380 (2005).
22. Couvillion, B. R., Beck, H., Schoolmaster, D. & Fischer, M. *Land Area Change in Coastal Louisiana (1932 to 2016). Map 3381* (U.S. Geological Survey, 2017); https://doi.org/10.3133/sim3381.
23. Nienhuis, J. H., Ashton, A. D., Roos, P. C., Hulscher, S. J. M. H. & Giosan, L. Wave reworking of abandoned deltas. *Geophys. Res. Lett.* **40**, 5899–5903 (2013).
24. Latrubesse, E. M. et al. Damming the rivers of the Amazon basin. *Nature* **546**, 363–369 (2017).
25. Yang, Z. et al. Dam impacts on the Changjiang (Yangtze) River sediment discharge to the sea: the past 55 years and after the Three Gorges Dam. *Water Resour. Res.* **42**, 04407 (2006).
26. Hoitink, A. J. F., Wang, Z. B., Vermeulen, B., Huismans, Y. & Kästner, K. Tidal controls on river delta morphology. *Nat. Geosci.* **10**, 637–645 (2017).
27. Dai, Z., Fagherazzi, S., Mei, X., Chen, J. & Meng, Y. Linking the infilling of the North Branch in the Changjiang (Yangtze) estuary to anthropogenic activities from 1958 to 2013. *Mar. Geol.* **379**, 1–12 (2016).
28. Jerolmack, D. J. & Swenson, J. B. Scaling relationships and evolution of distributary networks on wave-influenced deltas. *Geophys. Res. Lett.* **34**, L23402 (2007).
29. Muto, T. & Swenson, J. B. Large-scale fluvial grade as a nonequilibrium state in linked depositional systems: theory and experiment. *J. Geophys. Res.* **110**, F03002 (2005).
30. Casas-Prat, M., Wang, X. L. & Swart, N. CMIP5-based global wave climate projections including the entire Arctic Ocean. *Ocean Model.* **123**, 66–85 (2018).
31. Dunn, F. E. et al. Projections of declining fluvial sediment delivery to major deltas worldwide in response to climate change and anthropogenic stress. *Environ. Res. Lett.* **14**, 084034 (2019).
32. Anthony, E. J. et al. Linking rapid erosion of the Mekong River delta to human activities. *Sci. Rep.* **5**, 14745 (2015).
33. Minderhoud, P. S. J. et al. The relation between land use and subsidence in the Vietnamese Mekong delta. *Sci. Total Environ.* **634**, 715–726 (2018).
34. Keogh, M. E. & Törnqvist, T. E. Measuring rates of present-day relative sea-level rise in low-elevation coastal zones: a critical evaluation. *Ocean Sci.* **15**, 61–73 (2019).

Methods

We predict delta morphology and delta morphologic change by calculating potential sediment transport fluxes due to waves, tides and the river. We obtain delta land area change by summing land gain and land loss from recent global surface-water change studies[20,35]. Our method involves the following seven steps, including estimates of uncertainty: (1) locating coastal river deltas globally, (2) obtaining the pristine and disturbed fluvial sediment flux for each delta, (3) calculating the wave-driven and (4) the tide-driven sediment flux for each delta, (5) producing a morphological prediction for each delta, (6) testing the morphological prediction and (7) obtaining rates of delta land area change.

Locating river deltas

We locate coastal deltas using HydroSheds at a resolution of 15 arcsec for all coasts south of 60° latitude[36]. HydroSheds uses hydrologically conditioned Shuttle Radar Topography Mission (SRTM)[37] data to generate gridded hydrologic data such as drainage direction and flow accumulation, and includes locations of river mouths globally.

The 15-arcsec HydroSheds dataset contains about 2.48 million first-order drainage basins; 85% of those are smaller than 1 km^2 (ref. [38]). Most of these small drainage basins have no river[38], and therefore also no delta. They appear mostly along coastlines because of elevation noise that leads to poor drainage delineation of flat, low-lying areas[39] (Extended Data Fig. 1). For studies that focus on rivers, a common solution to this problem is to limit the analysis to drainage basins larger than a certain size (for example, 40,000 km^2)[14]. Unfortunately, this solution is not appropriate for our purposes because it would exclude many of the smaller deltas. Instead, we select river mouths with a drainage area of at least 50 km^2 if it contains a drainage divide higher than 40 m above mean sea level. We also include drainage basins larger than 1,000 km^2 regardless of the drainage basin topography. Accounting for drainage area elevations in small basins allows us to exclude most of the coastal noise caused, for example, by vegetation, but still captures many small, mountainous drainage basins. We find drainage divide elevations for all river mouths from our initial selection by extracting the SRTM elevation along each drainage basin boundary (Extended Data Fig. 1).

For latitudes greater than 60°, where HydroSheds is not available, we find deltas by selecting drainage basins larger than 1,000 km^2 based on the 1-min ETOPO1[40] grid, which is available globally. We eliminate non-coastal deltas by only selecting potential delta-mouth locations closer than 12 arcmin to the National Oceanic and Atmospheric Administration (NOAA) shoreline (~15 km, depending on the latitude)[41].

To further improve our dataset and include only alluvial river mouths, we use the WBMSED 2.0 distributed global-scale sediment flux model[14,42] and retrieve river discharge and sediment flux for each river mouth (see Methods section 'Fluvial sediment flux Q_{river}'). We remove river mouths with a river discharge below 1 m^3 s^{-1} or a sediment flux below 0.01 kg s^{-1} (arid environments). We use the global coastal typology dataset of Dürr et al.[43] to further remove drainage basins smaller than 1,000 km^2 that drain into fjords, where R and T are unlikely to be appropriate indicators of their morphology. Our resulting dataset consists of 10,848 deltas on all major landmasses except Antarctica and Greenland.

We investigate whether our criteria lead to the inclusion of most coastal deltas globally by creating a test dataset of deltas on Madagascar. Madagascar has a wide range of wave exposure, tidal amplitudes and, consequently, coastal environments. Using 1-m-resolution DigitalGlobe images we visually identify 306 river mouths, of which 236 appear deltaic (where the coastal morphology is affected by the presence of a river; see .kml file at https://doi.org/10.17605/OSF.IO/S28QB). Of the 236 deltas, our algorithm finds 212, and 24 deltas were

not located (false negatives, generally small deltas). Our dataset also includes 12 drainage basins that do not have a delta (false positives); these tend to be tributaries to other rivers with confluences near the coast, or small drainage basins without an observable river. We include bayhead deltas in our dataset.

Our test dataset allows us to compute the uncertainty on the global number of deltas (Extended Data Table 1). Combined, our assessment indicates an accuracy of 85%. By extrapolating globally outside Madagascar and following Olofsson et al.[44], we obtain a standard deviation of 252 and 95% confidence bounds of ±494. Because our false-negative and false-positive rates are comparable, our estimate of 10,848 coastal deltas is unlikely to be strongly biased[44].

Fluvial sediment flux Q_{river}

To estimate the fluvial sediment flux for every delta, we use the WBMSed 2.0 distributed global-scale sediment flux model[14,42]. WBMSed is an empirical model that calculates gridded daily fluvial water discharge on the basis of precipitation, temperature, soil type, elevation and other datasets, in this case for the years 1980–2010. Sediment discharge is then estimated using the BQART model[45].

WBMSed is available globally at a resolution of 6 arcmin, which is lower than that of the HydroSheds data. We therefore convert the WBMSed accumulated discharge and sediment flux file to a discharge and sediment yield (Extended Data Fig. 2). We then sum the discharge and sediment yield across the drainage basins to calculate a discharge and Q_{river} for each delta.

WBMSed accounts for human influences on fluvial sediment fluxes by including empirically tested trapping coefficients for river dams and human erosion parameters to account for land-use changes. By disabling these coefficients, WBMSed can estimate fluvial sediment fluxes for a world without humans[42]. We use 'pristine' (without humans) and 'disturbed' (with humans) model results from Cohen et al.[42] to investigate human-induced changes to delta morphology (Extended Data Fig. 3). We note that depending on the history of anthropogenic change, pristine conditions can refer to different time periods, depending on the drainage basin. The Mekong River Delta, for example, has had a long history of human impact on its fluvial sediment flux[46]. Disturbed conditions refer to the present day and include the effects of afforestation and improved soil conservation practices on the fluvial sediment flux to river deltas. WBMSed is validated by independent measurements of the fluvial sediment flux of pristine and disturbed drainage basins[42]. We note that both realizations are based on the 1980–2010 hydroclimate, so we exclude the effects of longer-term climate change on the fluvial sediment flux.

WBMSed provides a reasonable prediction of sediment discharge as tested against observations ($R^2 = 0.66$)[14]. Sediment flux estimates remain challenging; therefore, predictions might differ from local case studies, both for pristine and for disturbed river basin conditions. WBMSed data should be considered estimates.

Wave sediment flux Q_{wave}

To assess ocean wave effects on delta morphology, we calculate the maximum potential alongshore sediment flux Q_{wave} (ref. [12]) for every delta using the NOAA WaveWatch III 30-year hindcast phase II[47] by extracting the angular distribution of the wave energy, the significant wave height and the wave period (Extended Data Fig. 4). The resolution of the wave data varies between 4 arcmin and 30 arcmin depending on location and bathymetric complexity. We extract the closest available wave data for each delta.

We calculate Q_{wave} by convolving the angular distribution of wave energy with an approximation of alongshore sediment transport recast into deep-water wave properties

$$Q_{wave} = \max_{-\pi \le \theta \le \pi} \left[E(\varphi_0) Q_s(\varphi_0 - \theta) \right] - \min_{-\pi \le \theta \le \pi} \left[E(\varphi_0) Q_s(\varphi_0 - \theta) \right] \qquad (1)$$

Article

where E (dimensionless) is the relative contribution of each wave approach angle φ_0 to alongshore sediment transport. Q_s (in kilograms per second) represents wave-driven alongshore sediment transport posed in deep-water terms as a function of the approach angle of the wave, φ_0, compared to the shoreline θ (refs. [12,48]). We do not have global data of shoreline orientation, and therefore calculate Q_{wave} by assuming maximum potential transport to the left and the right, away from the river mouth[12]. Given that most of the wave energy is directed towards the coast (not away from the coast), this is unlikely to be a major component of the uncertainty.

Our analysis assumes that waves refract and shoal over shore-parallel contours[12,48] and that the delta is exposed to waves from all directions. Complex nearshore bathymetry and shadowing by headlands can have a considerable effect on wave transformations, but cannot be accounted for in this global model. We therefore assume that if wave data are found within 1° of the river mouth, the delta is not sheltered from wave attack. We assume negligible wave-driven sediment transport if the delta is located farther than 1° from available wave data (sheltered, mostly bayhead deltas). This cutoff could falsely identify some bayhead deltas as wave-dominated, whereas other open-coast deltas might be labelled river-dominated owing to the coarse WaveWatch III grid resolution. we note that this is an important simplification that should be improved upon in the future.

The fluvial dominance ratio R compares the wave-driven flux Q_{wave} to the fluvial sediment that is retained nearshore. WBMSed predicts fluvial suspended load sediment fluxes, of which a large fraction will probably be lost to the marine environment. Bedload fluxes are more likely to be retained nearshore, but no global data exist to predict these fluxes. Here we assume that WBMSed approximates the fluvial sediment load that is retained nearshore. This assumption will most probably lead to an underestimation of wave dominance for larger, suspended-load dominated rivers and an overestimation of wave dominance for smaller, bedload dominated rivers.

The fluvial dominance ratio R is dependent on the number of distributary channels. The potential alongshore transport Q_{wave} acts on each river mouth, whereas Q_{river} is split between river mouths[12]. Because no global data on distributary channel networks exist we neglect the effect of distributary formation on Q_{wave}, and therefore might underpredict wave influence on deltas with multiple distributaries (for example, Mekong Delta[49]).

Tidal sediment flux Q_{tide}

We calculate Q_{tide} for every coastal delta to establish the effect of tides on delta morphology. Q_{tide} is a tidal sediment flux amplitude at the mouth of a delta. If Q_{tide} is large compared to Q_{river}, we predict considerable channel widening compared to the upstream (fluvial) channel width. Q_{tide} requires estimates of the tidal amplitude, angular frequency, channel cross-sectional aspect ratio and channel slope[13]. We extract the tidal amplitude and angular frequency of 13 tidal constituents globally for all deltas using the 15-arcsec-resolution OSU TOPEX dataset[50] (Extended Data Fig. 5). We define the mean tidal amplitude as half of the sum of all tidal constituents and use either a semi-diurnal or a diurnal frequency, depending on the delta location.

We estimate the channel slope from the HydroSheds accumulated drainage area data (ACC files)[36] and the global SRTM data[37] by tracking the elevation upstream from every delta up to 20 m above the mean sea level (Extended Data Fig. 1b). We then fit an exponential function to the elevation data and calculate the gradient of that function at sea level[13]. We assume a slope of 1×10^{-3} (median slope of all coastal deltas) if SRTM elevation data are missing (>60° latitude) or if its resolution is insufficient to capture the water-surface elevation of deltas.

Nienhuis et al.[13] defined tidal dominance as the ratio of tidal discharge amplitude ($Q_{w,tide}$, in cubic metres per second) and the mean annual river discharge ($Q_{w,river}$, in cubic metres per second). To compare tidal dominance to wave dominance, here we define an equivalent tidal sediment flux Q_{tide} by assuming that the sediment concentration of the tidal discharge is equal to the sediment concentration of the river discharge. We estimate Q_{tide} as

$$Q_{tide} = Q_{w,tide} \frac{Q_{river}}{Q_{w,river}} \tag{2}$$

such that the ratio T in discharge terms is equivalent to the ratio posed in sediment fluxes. We calculate $Q_{w,tide}$ by

$$Q_{w,tide} = \frac{1}{2}\omega k a^2 \left(\frac{d_u}{S}\right)^2 \beta \tag{3}$$

where ω is the tidal angular velocity (s^{-1}); k is a proportionality coefficient (m^{-1}) that is dependent on the grain size, Shields stress and flow roughness[13]; a is the mean tidal amplitude (m) (Extended Data Fig. 5); d_u is the upstream channel depth (m); S is the channel slope; and β is the channel aspect ratio. We estimate the aspect ratio and depth of each river based on its discharge following hydraulic geometry[16]. Q_{tide} has been tested for a broad selection of deltas globally and was found to be an appropriate indicator of tidal dominance in a broad range of wave environments[13].

Combining Q_{river}, Q_{tide} and Q_{wave}

To estimate the location of deltas within a ternary diagram we determine the fraction r of the total sediment flux contributed by waves, tides and the river

$$r_x = \frac{Q_x}{Q_{river} + Q_{wave} + Q_{tide}} \tag{4}$$

where x represents river, wave or tide. The relative sediment flux r can vary between 0 and 1, whereas the river- and tidal-dominance ratios R and T vary between $1/\infty$ and ∞ (Fig. 1a, b). r allows us to uniquely position a river delta within the ternary diagram and characterize its two first-order morphological indicators, the delta protrusion angle and the channel width divergence. Similarly to wave, tide and river dominance, a delta is considered tide-dominated if Q_{tide} exceeds both Q_{river} and Q_{wave}. By assessing Q_{river}, Q_{tide} and Q_{wave} for all deltas globally, we find that 8,551 (79%) are wave-dominated, 1,170 (11%) are river-dominated and 1,127 (10%) are tide-dominated.

Accuracy of delta morphology prediction

To test our predictions of delta morphology, we analysed 212 deltas on Madagascar, supplemented by 100 deltas picked randomly from our dataset, and visually categorized them as river-, wave- or tide-dominated (Extended Data Table 2). Following Olofsson et al.[44], we obtain prediction accuracies of 91%, 55% and 64%, for wave-, river- and tide-dominated deltas, respectively, which indicate the likelihood that any one particular delta is classified correctly (equation 2 in ref. [44]). By weighting by their occurrence, we obtain an overall accuracy of 85% (±2%, determined through bootstrapping) (equation 4 in ref. [44]). By correcting for the size of the dataset, we obtain estimates of the 95% confidence interval of the global fraction of wave-, river- and tide-dominated deltas of 79% ± 9%, 11% ± 2%, and 10% ± 3%, respectively (equation 11 in ref. [44]).

We note that although the island of Madagascar has a large variety of coastal landforms, it is not necessarily a good statistical representation of coastlines worldwide. Our morphological accuracy assessment is therefore biased, and we do not adjust the gross total proportion of river-, wave- or tide-dominated deltas on the basis of our visual assessment.

Measurements of recent deltaic change

We measure the deltaic surface area change by combining our dataset of river mouths and their associated deltas with surface-water changes

between 1985 and 2015 mapped on a global scale by the Aqua Monitor[20]. To select the appropriate coastal change per delta we first determine delta extents along the NOAA vectorized shoreline dataset[41]. Next, we use an empirical approximation of the delta area[51], ~$1.07(Q_{river}^{1.1} Q_{w,river}^{0.45})/D_{sh}$ (in square kilometres), where $Q_{w,river}$ is the river discharge and D_{sh} is the shelf depth, here $D_{sh} \approx 100$ m (ref. [51]). We obtain a delta radius (~(area/π)$^{1/2}$), set a minimum radius of 2 km for small deltas, and match every shoreline location within the radius of that particular delta (Extended Data Fig. 5). Using Google Earth Engine[52], we then retrieve local surface-water changes along these deltaic coastlines, summing land gain and land loss along the NOAA vectorized shorelines within a buffer equal to one-tenth of the delta radius (Extended Data Fig. 5). The NOAA shorelines include banks of wide coastal channels such as estuaries. By selecting only land area change near the NOAA shorelines, we exclude land–water conversion within delta interiors (away from channel banks and shorelines), for which R and T are not appropriate indicators. Land area change resulting from, for example, subsidence, tectonic activity, or delta plain engineering, is therefore probably not fully captured in our reported delta-area change. Land area change of abandoned delta lobes near active parts of the delta might be included. We note the potential for sizeable anthropogenic effects on land gain and land loss (for example, land reclamation), and therefore mask out portions of each delta that are classified as urban/artificial (class 190) areas by the GlobCover[53] dataset.

We estimate the uncertainty in the land gain and land loss measurements by combining three sources of error. The first source of error lies in the per-pixel classification of water versus land. The Global Surface Water Explorer reports uncertainty of about 1% in their classification[35]. The Aqua Monitor uses a similar classification algorithm and therefore probably has similar uncertainty. The second source of error is the categorization of changes in the water-to-land and land-to-water transition. We estimate this uncertainty by comparing deltaic land area changes between the AquaMonitor[20] and the Global Surface Water Explorer[35], which use different algorithms to classify transitions. We obtain a covariance of 7%, which we include as a measure of the spatial uncertainty.

A third source of uncertainty is the shoreline length and buffer assigned to every delta, and how much of the change within and outside that area is related to delta morphodynamics. To quantify this uncertainty, we manually map the surface extents of 40 deltas in Madagascar and measure land surface changes within those deltas. A comparison with automatically mapped areas yields a standard error of 1%. We combine the three sources of uncertainty and obtain a standard error of the mean of 9% per delta. The total net deltaic land area change ±2 s.d. for the 10,848 deltas in the dataset between 1985 and 2015 is 54 ± 12 km^2.

Aside from a global assessment, we also compare land gain rates of specific deltas to values reported by case studies in the literature (Extended Data Table 5). For the Mississippi Delta comparison, we therefore include land loss rates of the 'birdfoot' area closest to the river mouth, as well as the Breton Sound basin as defined by Couvillion et al.[22]. For the seven deltas considered, the global analysis seems to capture delta land loss and land gain in the same order of magnitude. Because the time periods and spatial coverages of these studies do not align, we use this only to illustrate similarities and differences between our reported land gain and earlier studies.

Data availability

All primary sources (OSU TOPEX[50], NOAA WaveWatch[47], USGS HydroSheds[36], USGS SRTM[37], WBMSed[42] and AquaMonitor[20] data) are publicly available. Wave and tide data can also be found at https://jhnienhuis.users.earthengine.app. The resulting morphological predictions for all 10,484 deltas are available as .mat and .kml files at https://doi.org/10.17605/OSF.IO/S28QB. Source data for Figs. 1–3 are provided with the paper.

Code availability

The Matlab computer code that reproduces our findings is available at https://github.com/jhnienhuis/GlobalDeltaChange and https://osf.io/s28qb/.

35. Pekel, J.-F., Cottam, A., Gorelick, N. & Belward, A. S. High-resolution mapping of global surface water and its long-term changes. *Nature* **540**, 418–422 (2016).
36. Lehner, B., Verdin, K. & Jarvis, A. New global hydrography derived from spaceborne elevation data. *Eos* **89**, 93–94 (2008).
37. USGS. Shuttle Radar Topography Mission. *Global Land Cover Facility, University of Maryland, College Park, Maryland* (USGS, 2006); https://www2.jpl.nasa.gov/srtm/.
38. Guth, P. L. Drainage basin morphometry: a global snapshot from the shuttle radar topography mission. *Hydrol. Earth Syst. Sci.* **15**, 2091–2099 (2011).
39. Rahman, M. M., Arya, D. S. & Goel, N. K. Limitation of 90 m SRTM DEM in drainage network delineation using D8 method—a case study in flat terrain of Bangladesh. *Appl. Geomatics* **2**, 49–58 (2010).
40. Amante, C. & Eakins, B. W. *ETOPO1 1 Arc-Minute Global Relief Model: Procedures, Data Sources and Analysis*. NOAA Technical Memorandum NESDIS NGDC-24 (NOAA, 2009).
41. NOAA. NOAA GSHHG Coastline (National Geophysical Data Center, 2015); http://www.ngdc.noaa.gov/mgg/shorelines/shorelines.html.
42. Cohen, S., Kettner, A. J., Syvitski, J. P. M. & Fekete, B. M. WBMsed, a distributed global-scale riverine sediment flux model: model description and validation. *Comput. Geosci.* **53**, 80–93 (2013).
43. Dürr, H. H. et al. Worldwide typology of nearshore coastal systems: defining the estuarine filter of river inputs to the oceans. *Estuaries Coasts* **34**, 441–458 (2011).
44. Olofsson, P. et al. Good practices for estimating area and assessing accuracy of land change. *Remote Sens. Environ.* **148**, 42–57 (2014).
45. Kettner, A. J. & Syvitski, J. P. M. HydroTrend v.3.0: a climate-driven hydrological transport model that simulates discharge and sediment load leaving a river system. *Comput. Geosci.* **34**, 1170–1183 (2008).
46. Wang, H. et al. Recent changes of sediment flux to the western Pacific Ocean from major rivers in East and Southeast Asia. *Earth Sci. Rev.* **108**, 80–100 (2011).
47. Chawla, A., Spindler, D. M. & Tolman, H. L. Validation of a thirty year wave hindcast using the Climate Forecast System Reanalysis winds. *Ocean Model.* **70**, 189–206 (2013).
48. Ashton, A. D. & Murray, A. B. High-angle wave instability and emergent shoreline shapes: 2. Wave climate analysis and comparisons to nature. *J. Geophys. Res.* **111**, F04012 (2006).
49. Tamura, T. et al. Origin and evolution of interdistributary delta plains; insights from Mekong River delta. *Geology* **40**, 303–306 (2012).
50. Egbert, G. D. & Erofeeva, S. Y. Efficient inverse modeling of barotropic ocean tides. *J. Atmos. Ocean. Technol.* **19**, 183–204 (2002).
51. Syvitski, J. P. M. & Saito, Y. Morphodynamics of deltas under the influence of humans. *Global Planet. Change* **57**, 261–282 (2007).
52. Gorelick, N. et al. Google Earth Engine: planetary-scale geospatial analysis for everyone. *Remote Sens. Environ.* **202**, 18–27 (2017).
53. Bontemps, S., Defourny, P., Bogaert, E. Van, Kalogirou, V. & Perez, J. R. *GLOBCOVER 2009 Products Description and Validation Report* (ESA & UCL, 2011).
54. Jiménez, J. A. & Sánchez-Arcilla, A. Medium-term coastal response at the Ebro delta, Spain. *Mar. Geol.* **114**, 105–118 (1993).
55. Hassan, S. M. T., Syed, M. A. & Mamnun, N. Estimating erosion and accretion in the coast of Ganges-Brahmaputra-Meghna Delta in Bangladesh. In *6th Int. Conference on Water & Flood Management* 115–124 (Institute of Water and Flood Management, 2017).
56. Sarwar, M. G. M. & Woodroffe, C. D. Rates of shoreline change along the coast of Bangladesh. *J. Coast. Conserv.* **17**, 515–526 (2013).
57. Kong, D. et al. Evolution of the Yellow River Delta and its relationship with runoff and sediment load from 1983 to 2011. *J. Hydrol.* **520**, 157–167 (2015).
58. Ali, E. M. & El-Magd, I. A. Impact of human interventions and coastal processes along the Nile Delta coast, Egypt during the past twenty-five years. *J. Aquat. Res.* **42**, 1–10 (2016).
59. Besset, M., Anthony, E. J. & Bouchette, F. Multi-decadal variations in delta shorelines and their relationship to river sediment supply: an assessment and review. *Earth Sci. Rev.* **193**, 199–219 (2019).

Author contributions J.H.N., A.D.A. and D.A.E. conceived the study. A.J.K. assisted with the global sediment flux calculations. J.H.N. carried out the study and wrote the initial draft. J.H.N., A.J.F.H. and T.E.T. discussed the results. All authors contributed to the writing of the manuscript.
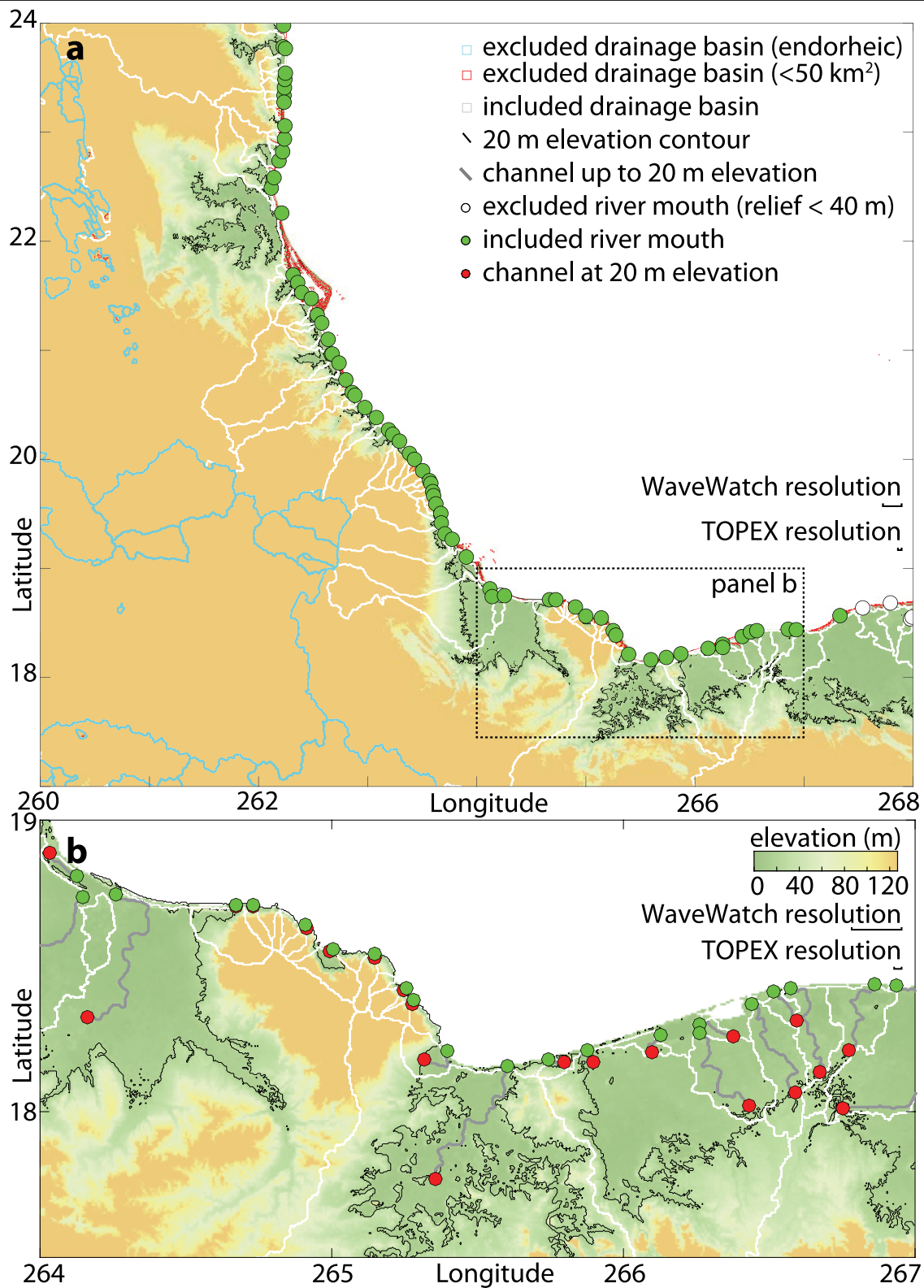
Extended Data Fig. 1 | Overview of the algorithm that identifies river deltas using HydroSheds data. a, HydroSheds drainage basins and the included deltas are shown for Veracruz, Mexico. **b**, Close-up of **a**, showing the included deltas and the tracked river channel for the channel slope calculation. Scale bars show the resolution of the WaveWatch[47] and TOPEX datasets[50].
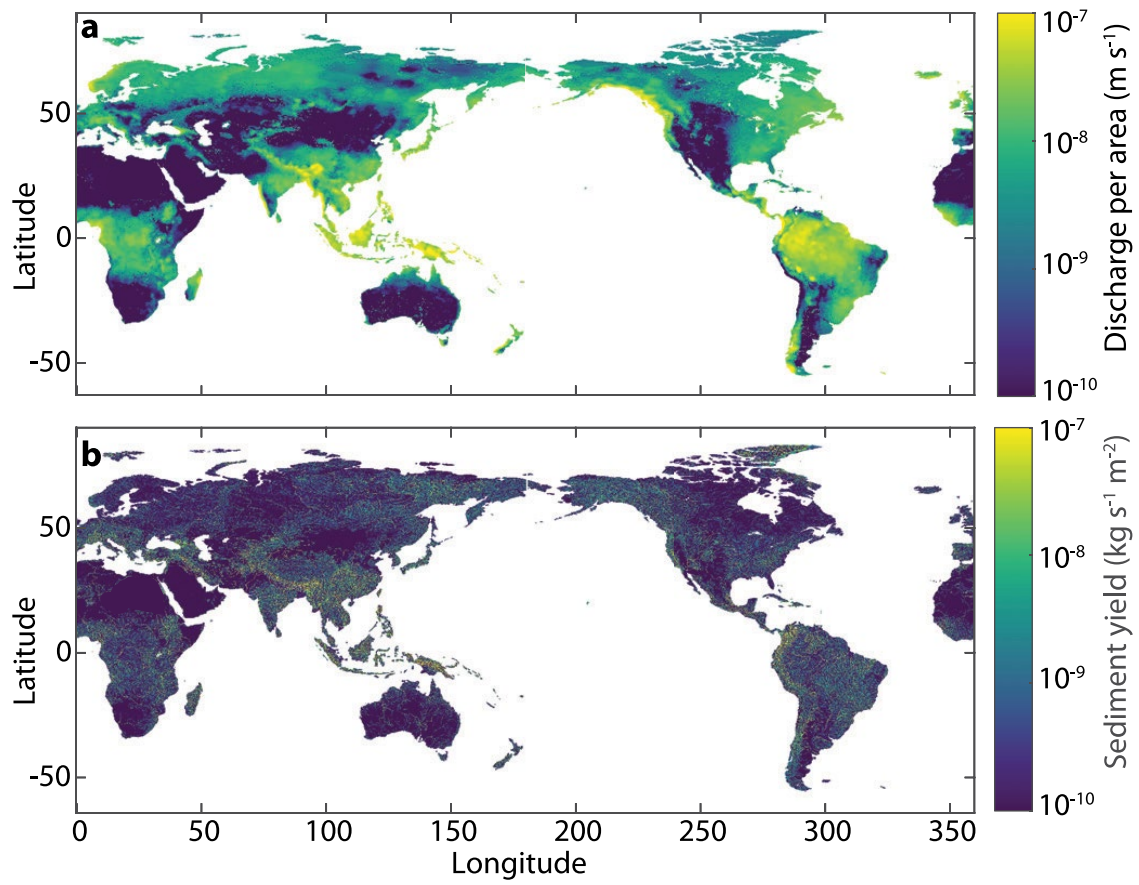
Extended Data Fig. 2 | WBMSed model predictions. a, Discharge per cell. **b**, Sediment yield[42].
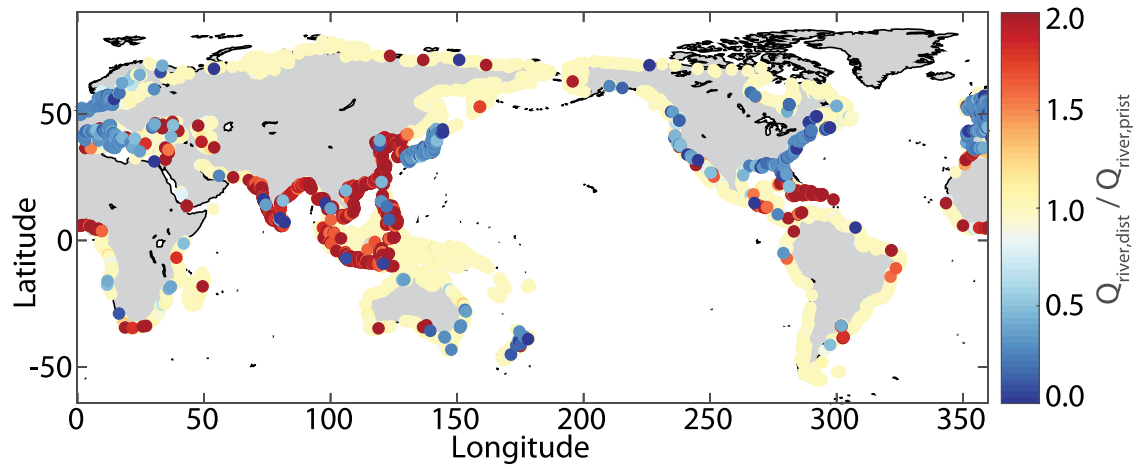
Extended Data Fig. 3 | WBMsed model predictions of human-induced change to the deltaic fluvial sediment flux. Colours indicate the ratio of the modern fluvial sediment flux (Q_{river}^{d}; here $Q_{river,dist}$) to the flux in a world without anthropogenic modifications[42] (Q_{river}^{p}; here $Q_{river,prist}$).
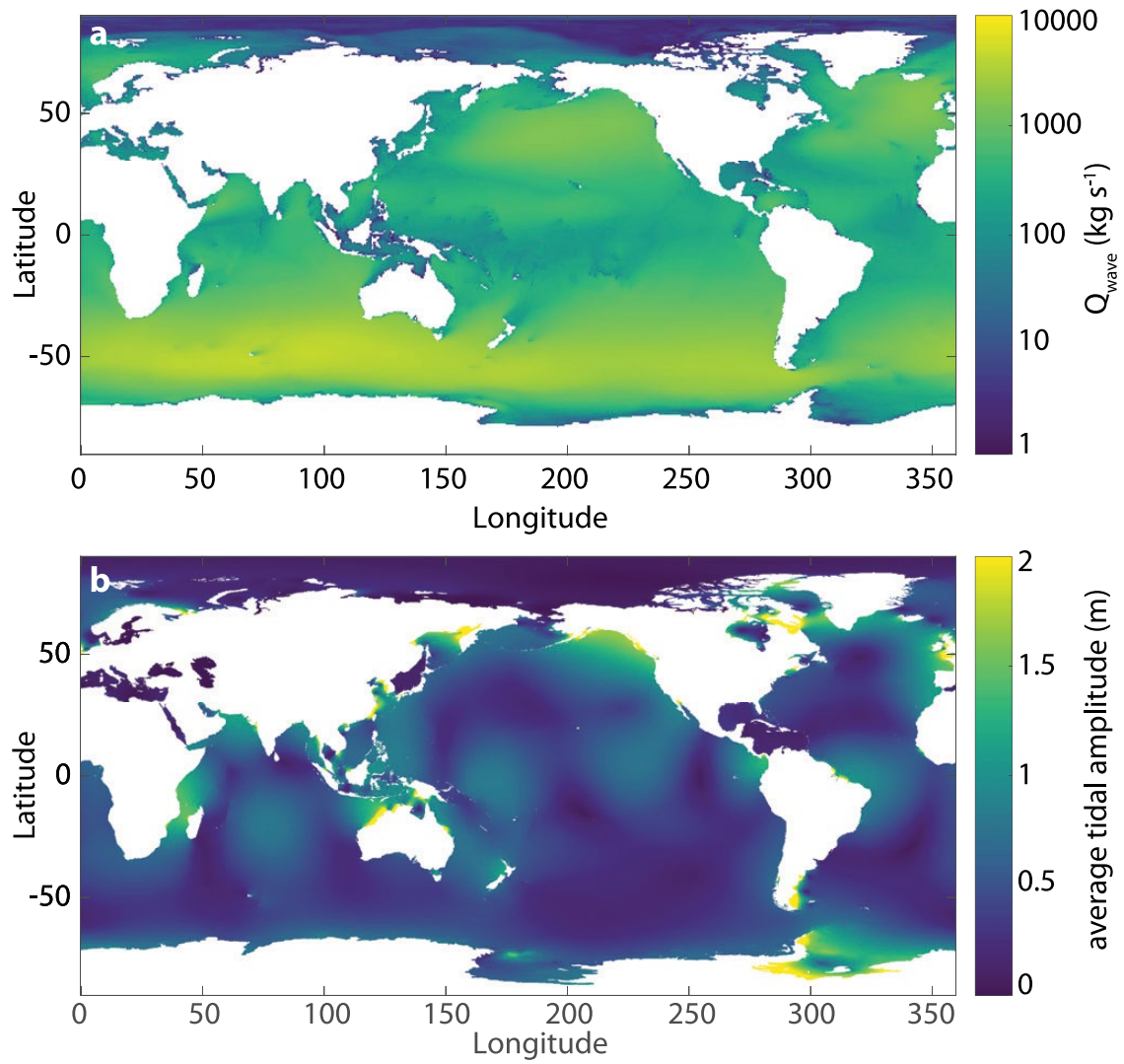
Extended Data Fig. 4 | Characterization of data used for wave- and tide-driven deltaic sediment flux. a, Global maximum potential alongshore sediment transport (Q_{wave}) based on the WaveWatch 30-year hindcast data[47]. **b**, Global estimate of mean tidal amplitude based on the OSU TOPEX data[50].
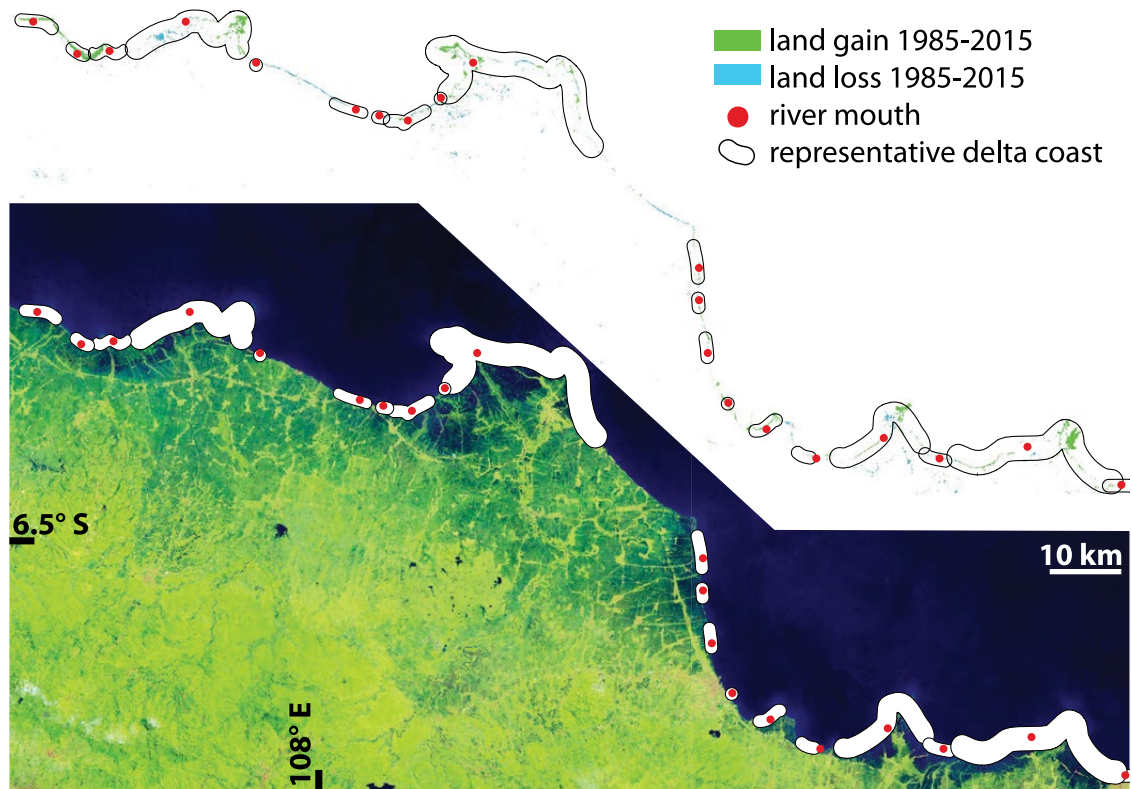
Extended Data Fig. 5 | Example of recent deltaic land area change for the north shore of Java, Indonesia. Land loss and land gain were measured using Landsat (http://landsat.usgs.gov/) images from Google Earth Engine[52] based on the Deltares Aqua Monitor[35]. Here, deltas have expanded recently because of human-induced increases in the fluvial sediment flux. The top image shows the coastal change, with the red markers and black outlines representing individual deltas and their coastlines, respectively.

Extended Data Table 1 | Confusion matrix of the number of deltas on Madagascar

		Observed	
		Delta	No delta
Predicted	Delta	212	12
	No delta	24	-

We note that the true-negative rate (no delta observed, no delta predicted) is infinite and therefore not included in our analysis.

Article

Extended Data Table 2 | Confusion matrix of the delta morphologic prediction based on a validation dataset of 312 deltas

		Observed (% of total)			
		Wave	River	Tide	Predicted total
Predicted (% of total)	Wave	72	3	8	83
	River	2	4	1	7
	Tide	1	0	9	10
	Observed total	74	8	18	100

Extended Data Table 3 | Yearly deltaic land gain, loss and net gain for different regions

	Land gain (km² yr⁻¹)	Land loss (km² yr⁻¹)	Net land gain (km² yr⁻¹)
Global	181 ± 8.3	- 127 ± 8.3	54 ± 11.8
East Africa	6 ± 1.6	- 3 ± 1.6	3 ± 2.3
South Asia	42 ± 1.7	- 32 ± 1.7	10 ± 2.4
West Africa	3 ± 1.3	- 3 ± 1.3	1 ± 1.8
Europe	10 ± 2.5	- 3 ± 2.5	8 ± 3.6
Central America	2 ± 1.8	- 1 ± 1.8	1 ± 2.5
Russia	1 ± 2.2	- 1 ± 2.2	0 ± 3.1
East Asia	34 ± 2.5	- 22 ± 2.5	11 ± 3.6
Northern Africa/Middle-East	5 ± 1.2	- 2 ± 1.2	3 ± 1.8
Eastern North America	6 ± 2.2	- 11 ± 2.2	- 4 ± 3.2
Western North America	2 ± 1.6	- 2 ± 1.6	0 ± 2.3
Oceania	6 ± 3.0	- 5 ± 3.0	1 ± 4.3
Eastern South America	33 ± 2.0	- 17 ± 2.0	16 ± 2.9
Western South America	3 ± 1.2	- 2 ± 1.2	2 ± 1.8
Southeast Asia	27 ± 4.2	- 23 ± 4.2	4 ± 5.9

Values represent averages from 1985 to 2015. Error limits indicate 2 s.d.

Article

Extended Data Table 4 | Predicted sediment transport fluxes for a selection of well-known deltas

Delta	River Water Discharge $Q_{w,river}$ (m³ s⁻¹)	Pristine Fluvial Sediment Flux Q^p_{river} (kg s⁻¹)	Disturbed Fluvial Sediment Flux Q^d_{river} (kg s⁻¹)	Wave-driven Sediment Flux Q_{wave} (kg s⁻¹)	Tide-driven Sediment Flux Q_{tide} (kg s⁻¹)	Net land gain (km² yr⁻¹)
Amazon	2.0E+5	3.8E+4	3.1E+4	2.9E-1	7.7E+5	1.0E+1
Arno	5.7E+1	7.0E+1	1.0E+0	1.7E+2	1.4E-1	2.1E-2
Colorado, MX	6.9E+2	3.8E+3	4.1E+0	2.9E+1	7.0E+3	-2.7E-1
Copper	1.2E+3	2.2E+3	3.4E+2	7.7E+2	2.8E+3	-7.1E-2
Danube	6.4E+3	2.1E+3	6.4E+2	2.3E+1	1.7E+1	3.7E-1
Ebro	1.4E+3	5.8E+2	2.8E+1	3.5E+1	4.0E+0	-3.8E-1
Eel, CA	2.4E+2	5.6E+2	7.5E+1	2.5E+3	1.5E+2	-1.7E-1
Elbe	4.2E+2	4.9E+2	2.5E+2	9.8E+0	4.1E+6	-2.7E-4
Ganges-Brahmaputra	3.1E+4	3.5E+4	3.5E+4	0.0E+0	2.0E+6	4.9E+0
Godavari	2.7E+3	5.4E+3	5.2E+3	3.8E+2	1.0E+2	5.0E-1
Huanghe	1.5E+3	3.5E+4	3.8E+3	2.3E+1	1.8E+1	-8.3E+0
Klamath	4.7E+2	3.2E+2	1.5E+2	2.4E+3	1.9E+3	1.2E-2
Lena	1.6E+4	6.3E+2	5.1E+3	1.2E+0	7.8E+2	7.1E-3
Mekong	1.7E+4	3.1E+3	3.0E+3	3.3E+1	4.0E+5	-2.1E-1
Mississippi	1.5E+4	1.3E+4	4.2E+3	1.0E+3	9.8E+2	-5.2E+0
Niger	6.1E+3	1.3E+3	8.0E+2	6.1E+2	4.8E+3	-4.9E-2
Nile	3.5E+3	3.8E+3	7.6E+1	2.2E+2	2.5E+2	-7.0E-1
Orange	4.4E+2	2.8E+3	3.0E+2	2.9E+3	1.1E+1	2.4E-1
Parana	1.5E+4	2.8E+3	2.5E+3	0.0E+0	9.0E+2	9.4E-1
Po	1.5E+3	5.5E+2	3.0E+2	4.2E+1	4.9E+2	1.2E-1
Rhine-Meuse	2.0E+3	2.0E+3	5.5E+2	1.2E+2	1.7E+4	6.5E-1
Rhone	1.7E+3	1.9E+3	5.6E+2	1.6E+2	7.9E+1	1.7E-1
Sao Francisco	3.6E+3	2.5E+3	1.7E+3	4.4E+3	1.7E+3	2.0E-2
Schelde	9.8E+1	1.9E+1	5.0E+0	6.8E+2	1.2E+0	3.2E-3
Senegal	6.9E+2	5.6E+2	4.3E+2	5.0E+2	8.9E+3	-4.7E-2
Volga	8.2E+3	6.0E+2	1.5E+3	0.0E+0	7.8E-1	3.8E+0
Yangtze	2.8E+4	1.5E+4	9.0E+3	6.1E+1	2.0E+4	-2.7E+0

See also Fig. 2b.

Extended Data Table 5 | Comparison of net land gain estimates with case studies from the literature

Delta	Net land gain ± 2 s.d. (km² yr⁻¹, this study)	Net land gain (km² yr⁻¹, other studies)	Study period	Source	Note
Ebro	-0.4 ± 0.2	-0.2	1957-1992	54	Based on shoreline transects
Ganges - Brahmaputra	4.9 ± 0.2	12.3	1973-2016	55	Hatiya and Bhola districts
Ganges - Brahmaputra	4.9 ± 0.2	0.4	1989-2009	56	Coastal Bangladesh
Huanghe	-8.2 ± 0.2	-4.0	1999-2011	57	Modern lobe
Mekong	-0.2 ± 0.2	0.5	2003-2012	32	Delta distributary mouths
Mississippi	-5.2 ± 0.2	-0.5	1985-2015	22	Birdfoot region
Mississippi	-5.2 ± 0.2	-15.0	1985-2015	22	Breton Sound basin
Nile	-0.7 ± 0.2	-0.2	1990-2014	58	
Parana	0.9 ± 0.2	2.0	1995-2015	59	

Case studies from refs. [22,32,54–59].